PHILOSOPHICAL MAGAZINE, 2003, VOL. 83, NO. 2, 245–276

Plastic slip distribution in two-phase laminate microstructures: dislocation-based versus generalized-continuum approaches

SAMUEL FOREST†

Ecole des Mines de Paris (CNRS), Centre des Matériaux (Unité Mixte de Recherche associée au CNRS 7633), BP 87, 91003 Evry Cedex, France

and RADAN SEDLÁČEK‡

Lehrstuhl für Werkstoffkunde und Werkstoffmechanik, Technische Universität München, Boltzmannstrasse 15, 85747 Garching, Germany

[*Received 11 February 2002 and accepted in revised form 18 July 2002*]

ABSTRACT

The size-dependent mechanical response of a simple model microstructure is investigated using continuum dislocation-based, Cosserat and strain-gradient models of crystal plasticity. The governing equations and closed-form analytical solutions for plastic slip and lattice rotation are directly compared. The microstructure consists of a periodic succession of hard (elastic) and soft (elastoplastic single-crystal) layers, subjected to single glide perpendicular to the layers. In the dislocation-based approach, inhomogeneous plastic deformation and lattice rotation are shown to develop in the soft channels, either because of bowing of dislocations or owing to pile-up formation. The generalized continuum non-local models are found to be able to reproduce the plastic slip and lattice rotation distribution. In particular, a correspondence was found between the generalized-continuum results and line tension effects; the additional or higher-order balance equations introduced in the non-local models turn out to be the counterparts of the equilibrium equation for bowed dislocations. The relevance and possible physical interpretation of additional or higher-order interface conditions responsible for the inhomogeneous distribution of plastic slip and lattice rotations are discussed.

§1. INTRODUCTION

In the current endeavour to connect the different scales involved in plasticity of metals from atomistics to continuum plasticity (Forest *et al*. 2001b), there is a strong research community trying to replace detailed descriptions of the collective behaviour of dislocations by continuum mechanical models. When the size of the investigated microstructure is of the order of magnitude of typically 1–10 μm, or below, classical continuum crystal plasticity theory, as described by Asaro (1983), for instance, ceases to be relevant since it is not able to reproduce the observed size effects. In contrast, non-local or generalized-continuum plasticity models incorpor-

† Email: samuel.forest@mat.ensmp.fr.
‡ Email: sedlacek@lam.mw.tu-muenchen.de.

Philosophical Magazine ISSN 1478–6435 print/ISSN 1478–6443 online © 2003 Taylor & Francis Ltd
http://www.tandf.co.uk/journals
DOI: 10.1080/0141861021000022255

ating intrinsic length scales account for the size effects, at least in a qualitative manner (Fleck and Hutchinson 1997).

The aim of the present work is to compare directly the governing equations and analytical solutions resulting from dislocation-based, Cosserat and strain-gradient models of crystal plasticity. For this purpose, a two-phase single-crystal material oriented for single slip and subjected to shear loading is investigated. A one-dimensional (1D) laminate microstructure consisting of periodically alternating layers of plastically soft and hard phases is considered. The hard phase is supposed to behave only elastically, and the soft channel as an elastic–ideally plastic material. Classical continuum crystal plasticity predicts homogeneous deformation and stress in each phase, possibly with a jump of some quantities at the interface. In contrast, the interest here is focused on the inhomogeneous distribution of plastic slip and lattice rotations in the soft phase arising from the analysis based on dislocation mechanics, as well as on Cosserat and strain-gradient continua. Intrinsic length scales which are responsible for size effects in plasticity of such layered microstructures arise naturally in the dislocation analysis. The present simple examples enlighten the importance and physical relevance of the additional boundary or interface conditions usually introduced in generalized plasticity models (Shu *et al.* 2001).

Comparisons between dislocation-based and strain-gradient models exist in the literature, at least in two-dimensional (2D) cases. Generally, results of 2D discrete dislocation dynamics are compared with non-local continuum models. For instance, Bassani *et al.* (2001) analysed the hardening behaviour induced by a periodic distribution of hard precipitates in a crystalline matrix oriented for single slip for the case of simple shear. For that purpose, dislocation dynamics is resorted to at the discrete level, whereas a non-local model is used at the continuum level. Localized or diffuse plastic deformation patterns resulting from the dislocation simulations are compared with the predictions of the non-local model. Shu *et al.* (2001) studied shearing of a single-crystal layer in detail for both single-slip and double-slip orientations. Dislocations are not allowed to cross the boundaries of the layer, which leads to inhomogeneous plastic deformation patterns. For both dislocation and continuum models, the analysis is based on numerical simulations, which makes it difficult to interpret clearly the continuum intrinsic length scales present in the model in terms of the corresponding elementary dislocation processes. In the present work, a very simple case is investigated in order to derive directly comparable closed-form solutions.

The dislocation simulations carried out by Cleveringa *et al.* (1998), Bassani *et al.* (2001) and Shu *et al.* (2001) are 2D in the sense that only straight dislocations in a plane perpendicular to them are considered. Formation of dislocation pile-ups and dipoles are then the most active elementary deformation and hardening mechanisms. However, the dislocations which are constrained to glide in the small volumes or narrow channels are generally required to bow out. Obviously, the bowing of dislocations cannot be taken into account in the 2D dislocation dynamics framework. By contrast, the continuum line-tension dislocation-based model presented in § 2 is able to account for the Orowan bowing which is frequently encountered in the plastic deformation of various dislocation substructures (cells, subgrains, ladders, etc.), single-crystal nickel-based superalloys, passivated thin films or microlaminates. The model to be presented here shows that the bowing of dislocations in the narrow channels leads to size effects. For completeness, an analysis of double-ended pile-ups of straight dislocations that can form in the soft channels under the considered

loading conditions is investigated in § 2.3. Pile-ups are usually regarded as an appropriate illustration of the dislocation accumulation at interfaces or grain boundaries. They classically illustrate the effect of the so-called geometrically necessary dislocations (Ashby 1970). As such, they have been the source of inspiration of several strain-gradient models. Both line-tension and pile-up dislocation-based models will be compared with the response of generalized-continuum models. A first attempt to identify directly the line-tension dislocation-based model with a Cosserat model has been presented by Sedláček and Forest (2000).

The Cosserat elastoplasticity model proposed in § 3 mimics the local response of the considered material in various situations, without explicitly introducing dislocation distributions. Analytical solutions under periodicity conditions are found and compared with the above dislocation approach. In particular, the circumstances under which the Cosserat rotation coincides with the lattice rotation are shown. Finally, in § 4, the plastic strain-gradient models given by Aifantis (1987, 1999), Fleck and Hutchinson (1997) and Shu and Fleck (1999) are recalled and applied to the present simple case to compare them with the dislocation and Cosserat models. It will be shown that the interface conditions to be fulfilled in each model play a major role in the modelling of inhomogeneous deformation patterns.

Throughout the paper, vectors and tensors are denoted by bold characters and index notation is used in the equations. The whole analysis is carried out within the small-strain and small-rotations framework.

§ 2. Dislocation models

Firstly, the line tension model presented by Sedláček and Forest (2000) is briefly reviewed and extended in the following two sections. Then, in § 2.3, an alternative configuration for which an explicit expression of dislocation distribution in the channels under shear is available, namely that of the double-ended pile-up, is briefly presented.

The considered periodic laminate microstructure with direction of the applied stress indicated and the coordinate system used is sketched in figure 1. Instead of individual dislocations, a continuous field of curved glide dislocations in the soft channel is considered. For simplicity, all quantities are assumed to be independent of y and z. The equilibrium position of a representative bowing screw dislocation $\varphi(x)$ with Burgers vector magnitude b and constant line tension T in a shear stress field $\tau(x)$ is considered:

$$\tau(x)b + T\,\partial_{xx}\varphi(x) = 0. \tag{1}$$

The second derivative of the dislocation displacement $\varphi(x)$ follows from the linearized dislocation curvature. Strictly speaking, the linearized dislocation model is restricted to anelasticity (bowing of dislocations in the soft phase) since it is unable to describe fully plastic flow, that is the glide of critically bowed dislocations depositing edge segments at the interfaces. To be able to deal with the plasticity, at least in an approximate way, one can introduce the Orowan stress in the soft channel of width s, $\tau_{\mathrm{Or}} \approx 1.5\mu b/s$, as a threshold stress; if the mean shear stress in the channel reaches the value of the Orowan stress, the dislocation shape no longer changes and the bowed-out dislocations glide in the channels, depositing edges at the interfaces. This transition from anelasticity to plasticity, which is introduced here in an *ad hoc* manner, arises naturally in the framework of the full-curvature model (Sedláček and Forest 2000, Sedláček *et al.* 2003).

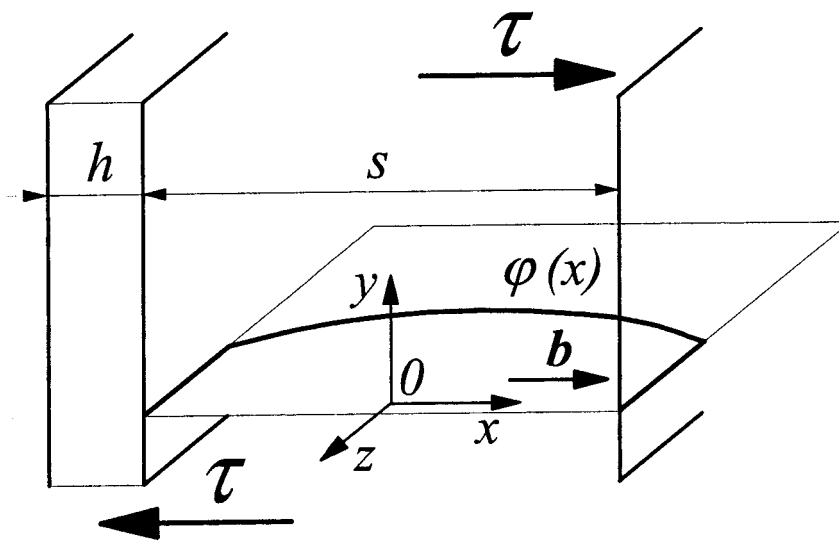

Figure 1. Dislocation bowing in the soft phase. A part of the loop gliding in the xOz plane is shown, with the curved (originally screw) section $\varphi(x)$ and edge segments at the soft–hard phase interface. The resolved shear stress τ and Burgers vector $\mathbf{b}$ are indicated. Labels s and h are used to designate the soft and hard phase respectively.

The increment of plastic shear caused by the displacement $\varphi(x)$ of the mobile dislocations with density ϱ_{m} follows from the Orowan relation

$$\gamma^{\mathrm{p}}(x) = \varrho_{\mathrm{m}} b \varphi(x). \tag{2}$$

The inhomogeneous plastic deformation is accommodated by the 'geometrically necessary' content of the bowing dislocations $\varphi(x)$ which is described by the Nye–Kröner dislocation density tensor $\boldsymbol{\alpha}$. Its only non-vanishing component $\alpha = \alpha_{xz}$ can be directly derived from the plastic shear:

$$\alpha(x) = \partial_x \gamma^{\mathrm{p}}(x). \tag{3}$$

It corresponds formally to continuously distributed 'pile-ups' of edge dislocations aligned with the z axis of figure 1, which is exactly the edge content of the bowing (originally screw) mobile dislocations with the scalar density ρ_{m}.

By utilizing Hooke's law for elastic shear strain $\varepsilon^{\mathrm{e}} = \varepsilon^{\mathrm{e}}_{xy}$,

$$\tau(x) = 2\mu\varepsilon^{\mathrm{e}}(x), \tag{4}$$

a differential equation for the elastic and plastic shear strains results:

$$2\varepsilon^{\mathrm{e}}(x) + \lambda^2 \, \partial_{xx}\gamma^{\mathrm{p}}(x) = 0, \tag{5}$$

with the intrinsic length scale λ given approximately by the average distance between the mobile dislocations:

$$\lambda = \left(\frac{T}{\mu \varrho_{\mathrm{m}} b^2} \right)^{1/2} \approx \frac{1}{\varrho_{\mathrm{m}}^{1/2}}. \tag{6}$$

We note in passing that the ratio s/λ of the channel width to the intrinsic length is crucial for the size effect appearing during plastic deformation of narrow channels, thin films, microlaminates, etc. (Sedláček and Forest 2000).

To be able to derive equations for the lattice rotation based on equation (5), relations for the elastic and plastic strains and rotations which will be extracted from the stress equilibrium and strain compatibility conditions are needed.

A compatible material displacement field $\mathbf{u} = (\bar{\gamma}y, u_y(x), 0)^{\mathrm{T}}$ is considered, leading to material displacement gradient, $\boldsymbol{\beta} = \operatorname{grad}\mathbf{u}$, of the form

$$\boldsymbol{\beta} = \begin{bmatrix} 0 & \bar{\gamma} & 0 \\ \partial_x u_y & 0 & 0 \\ 0 & 0 & 0 \end{bmatrix}. \tag{7}$$

The inhomogeneous plastic shear (2) causes a generally incompatible plastic distortion

$$\boldsymbol{\beta}^{\mathrm{p}} = \gamma^{\mathrm{p}}\mathbf{s} \otimes \boldsymbol{\nu} = \begin{bmatrix} 0 & \gamma^{\mathrm{p}} & 0 \\ 0 & 0 & 0 \\ 0 & 0 & 0 \end{bmatrix}. \tag{8}$$

The slip direction $\mathbf{s}$ and the normal $\boldsymbol{\nu}$ to the slip plane coincide with axes x and y respectively (see figure 1). Finally, the elastic distortion $\boldsymbol{\beta}^{\mathrm{e}} = \boldsymbol{\beta} - \boldsymbol{\beta}^{\mathrm{p}}$ results in the form

$$\boldsymbol{\beta}^{\mathrm{e}} = \begin{bmatrix} 0 & \gamma^{\mathrm{e}} & 0 \\ \partial_x u_y & 0 & 0 \\ 0 & 0 & 0 \end{bmatrix}, \tag{9}$$

where $\gamma^{\mathrm{e}}(x) = \bar{\gamma} - \gamma^{\mathrm{p}}(x)$. The symmetric part of $\boldsymbol{\beta}^{\mathrm{e}}$ determines the elastic strain which enters Hooke's law (4):

$$\varepsilon^{\mathrm{e}}(x) = \frac{\gamma^{\mathrm{e}} + \partial_x u_y}{2}. \tag{10}$$

The skew-symmetric part of $\boldsymbol{\beta}^{\mathrm{e}}$ can be represented by the axial vector $\boldsymbol{\phi}^{\mathrm{e}} = (0, 0, \phi^{\mathrm{e}} = \phi^{\mathrm{e}}_z)^{\mathrm{T}}$ of lattice rotation:

$$\phi^{\mathrm{e}}(x) = -\frac{\gamma^{\mathrm{e}} - \partial_x u_y}{2}. \tag{11}$$

To solve the boundary value problem outlined here, a homogeneous strain and a homogeneous stress approximation are considered successively. These two cases are treated in §§ 2.1 and 2.2.

2.1. *Isostrain approximation*

In homogenization theory, this isostrain approximation is referred to as the Voigt or Taylor model. In materials science, it goes by the name of the composite model (Mughrabi 1983). Here not only compatibility of deformation is required, but also homogeneity in material shear strain,

$$\gamma^{\mathrm{e}}(x) + \gamma^{\mathrm{p}}(x) = \bar{\gamma}, \quad \partial_x u_y = 0, \tag{12}$$

where $\bar{\gamma}$ is a homogeneous applied shear strain. To allow for a non-trivial solution, one has to relax the stress equilibrium ($\operatorname{div}\boldsymbol{\sigma} = 0$) by allowing for internal stresses. The inhomogeneous shear stress averaged over a period $s + h$ equals the applied shear stress $\bar{\tau}$ (the so-called Albenga law):

$$\bar{\tau} = \frac{1}{s+h}\left(\tau_h h + \int_{\langle s\rangle} \tau_s(x)\,\mathrm{d}x\right). \tag{13}$$

The equation governing distribution of lattice rotation in the soft phase follows immediately from equations (5), (11) and (12). Thus

$$\phi_s^{\mathrm{e}}(x) - \lambda^2\,\partial_{xx}\phi_s^{\mathrm{e}}(x) = 0. \tag{14}$$

Lattice rotation in the hard phase results from equations (4), (10) and (11), (12):

$$\phi_h^{\mathrm{e}} = -\frac{\tau_h}{2\mu}, \tag{15}$$

where τ_h is the shear stress in the hard phase determined from equation (13).

As for boundary conditions, in the anelastic regime, that is when $((1/s)\int_{\langle s\rangle}\tau_s(x)\,\mathrm{d}x < \tau_{\mathrm{Or}})$, continuity of lattice rotation is required. In the plastic regime, when $((1/s)\int_{\langle s\rangle}\tau_s(x)\,\mathrm{d}x = \tau_{\mathrm{Or}})$, there is a discontinuity of the lattice rotation caused by the discontinuity of the plastic strain accommodated by the edge dislocation segments at the interfaces. The magnitude of plastic strain is governed by internal stresses, that is by kinematic hardening (cf. equation (13)). Solutions to the above equations are of cosh type and are given explicitly by Sedláček and Forest (2000).

Since the homogeneity of material shear strain (equation (12)), is a stronger requirement than the compatibility of material distortion, the 1D isostrain approximation overestimates the magnitude of internal stresses.

2.2. *Isostress solution*

In homogenization theory, the isostress approximation is referred to as the Reuss or static model. In fact, in the present simple case, it is the exact solution of the continuum mechanics and dislocation balance equations. Stress equilibrium ($\mathrm{div}\,\boldsymbol{\sigma} = 0$) requires that the shear stress is constant and equal to the applied shear stress:

$$\tau(x) = \bar{\tau}. \tag{16}$$

With Hooke's law (4) in the form

$$\varepsilon^{\mathrm{e}} = \frac{\bar{\tau}}{2\mu}, \tag{17}$$

equation (5) yields the following equation for the plastic shear strain:

$$\lambda^2\,\partial_{xx}\gamma^{\mathrm{p}}(x) = -\frac{\bar{\tau}}{\mu}. \tag{18}$$

Because the soft phase is elastic–ideally plastic and from the discussion following equation (1), it is clear that $\bar{\tau} \leqslant \tau_{\mathrm{Or}}$. To obtain a unique solution to the problem at $\bar{\tau} = \tau_{\mathrm{Or}}$ (plastic regime), one has to fix the mean material strain by requiring, for example, for the mean applied material shear strain that

$$\frac{\bar{\gamma}}{2} = \frac{1}{s+h}\left(\bar{\varepsilon}_h h + \int_{\langle s\rangle} \varepsilon_s(x)\,\mathrm{d}x\right). \tag{19}$$

Without such a requirement, the amount of plastic deformation and rigid-body rotation would remain undetermined. This is quite different from the complementary case of the isostrain approximation (§ 2.1) where the amount of plastic deformation

has been determined by the amount of kinematic hardening and, owing to the internal stresses, $\bar{\tau} > \tau_{\mathrm{Or}}$ has been by all means admissible. From equations (7), (10), (17) and (19), the amount of plastic deformation can be found:

$$\int_{\langle s \rangle} \gamma^{\mathrm{p}}(x)\,\mathrm{d}x = \left(\bar{\gamma} - \frac{\bar{\tau}}{\mu}\right)(s+h). \tag{20}$$

The lattice rotation can be obtained from equations (10), (11) and (17) as

$$\phi^{\mathrm{e}}(x) = \frac{\bar{\tau}}{2\mu} - \bar{\gamma} + \gamma^{\mathrm{p}}(x). \tag{21}$$

As a consequence of equation (21), $\partial_x \gamma^{\mathrm{p}} = \partial_x \phi^{\mathrm{e}}$, and the governing equation for the lattice rotation in the soft phase ϕ_s^{e} becomes

$$\lambda^2\, \partial_{xx}\, \phi_s^{\mathrm{e}}(x) = -\frac{\bar{\tau}}{\mu}. \tag{22}$$

Accordingly, the lattice rotation and plastic slip (equation (18)) display a parabolic profile,

$$\phi_s^{\mathrm{e}}(x) = ax^2 + bx + c, \tag{23}$$

with $a = -\bar{\tau}/2\lambda^2\mu$. Note that, in the isostress framework, the exact solution of the full-curvature problem is well known; it is a circular arc. Nevertheless, we have linearized the curvature in equation (1), to be consistent with the rest of the paper. From symmetry reasons (periodicity),

$$\partial_x \phi^{\mathrm{e}}(0) = 0, \tag{24}$$

which implies that $b = 0$. In the anelastic regime ($\bar{\tau} < \tau_{\mathrm{Or}}$), the requirement for continuity of lattice rotation,

$$\phi_s^{\mathrm{e}}\left(\pm\frac{s}{2}\right) = \phi_h^{\mathrm{e}}, \quad \bar{\tau} < \tau_{\mathrm{Or}}, \tag{25}$$

determines the constant c. Lattice rotation in the hard phase results from equation (21):

$$\phi_h^{\mathrm{e}} = \frac{\bar{\tau}}{2\mu} - \bar{\gamma}. \tag{26}$$

Accordingly, the solution takes the form

$$\phi_s^{\mathrm{e}}(x) = \left(\frac{\bar{\tau}}{2\mu} - \bar{\gamma}\right) - \frac{\bar{\tau}}{2\mu}\left(\frac{x^2}{\lambda^2} - \frac{s^2}{4\lambda^2}\right), \quad \bar{\tau} < \tau_{\mathrm{Or}}. \tag{27}$$

In the plastic regime ($\bar{\tau} = \tau_{\mathrm{Or}}$), there is a discontinuity of the lattice rotation, $\Delta\phi^{\mathrm{e}}$, caused by the discontinuity of the plastic strain, $\Delta\gamma^{\mathrm{p}}$, which is accommodated by the edge dislocations deposited at the interfaces. The solution is:

$$\phi_s^{\mathrm{e}}(x) = \left(\frac{\bar{\tau}}{2\mu} - \bar{\gamma}\right) - \frac{\bar{\tau}}{2\mu}\left(\frac{x^2}{\lambda^2} - \frac{s^2}{4\lambda^2}\right) + \Delta\phi^{\mathrm{e}}, \quad \bar{\tau} = \tau_{\mathrm{Or}}. \tag{28}$$

The magnitude of the discontinuity $\Delta\phi^{\mathrm{e}}$ is determined from equations (20) and (21):

$$\Delta\phi^{\mathrm{e}} = \frac{s+h}{s}\left(\bar{\gamma} - \frac{\bar{\tau}}{\mu}\right) - \frac{\bar{\tau}}{12\mu}\frac{s^2}{\lambda^2}. \tag{29}$$

We shall return to the meaning of the step in lattice rotation later in the text.

Even though the stress equilibrium and strain compatibility are fulfilled exactly in the 1D isostress framework, the model is not realistic enough, for it cannot account for the internal stresses (i.e. kinematic hardening) which would arise in 2D or three-dimensional (3D) structures. In the 1D model, the internal stresses are fully relaxed by the lattice rotations.

2.3. *Pile-up model*

This section presents a different model of dislocation structure that can form under the same applied loading conditions and that leads to a 1D distribution of plastic slip in the macroscopic limit, that is dislocation pile-ups. This model is often advocated for the motivation of non-local theories and is recalled here, although its ingredients are different from the models in § 2 based on line tension effects.

A configuration for which an explicit expression of dislocation distribution in the channels under shear is available is that of the double-ended pile-up (Tanaka and Mura 1981, Hirth and Lothe 1982), caused by the simple shearing of a single Frank–Read source at the centre of the channel of width s (figure 2). A refinement of this theory has been given by Friedman and Chrzan (1998) taking in particular the extension of the source into account. For simplicity, we take $h \approx 0$ so that any image force due to the presence of the hard phase h acting on dislocations in the

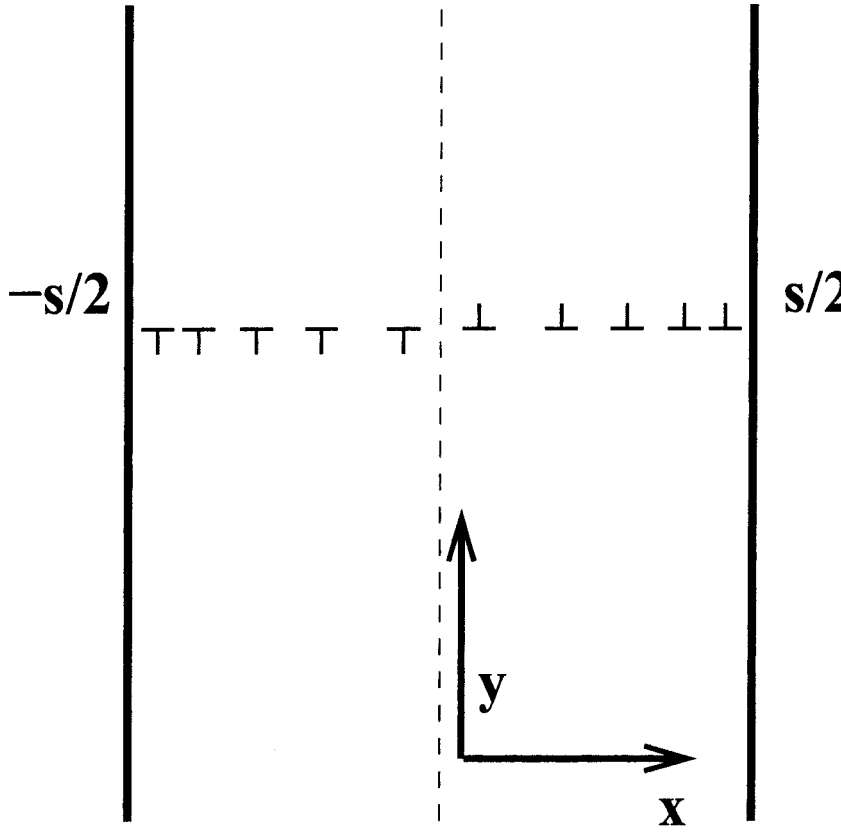

Figure 2. Double-ended dislocation pile-up in the soft phase under simple shear.

channel can be neglected. The approach based on the continuum theory of dislocations is briefly recalled here, in the case of pile-ups of edge dislocations with a Burgers vector of magnitude b. The equilibrium of dislocations under the applied stress $\bar{\tau}$ can be written

$$\bar{\tau} + \tau_{\mathrm{d}} + \tau_{\mathrm{c}} = 0, \tag{30}$$

where τ_{d} is the stress at x due to all present dislocations and τ_{c} the (assumed constant) threshold for the onset of dislocation motion. If $n(x)$ denotes the number of dislocations per unit length, the dislocation stress takes the form

$$\tau_{\mathrm{d}}(x) = A \int_{-s/2}^{s/2} \frac{n(x')}{x - x'} \, \mathrm{d}x',$$

with

$$A = \frac{\mu b}{2\pi(1-\nu)}. \tag{31}$$

A solution $n(x)$ of the integral equation (30) exists under the condition of unbounded density at two tips of the pile-up, namely $x = \pm s/2$ in figure 2:

$$n(x) = \frac{\bar{\tau} - \tau_c}{\pi A} \frac{x}{[(s/2)^2 - x^2]^{1/2}}. \tag{32}$$

The total number of dislocations in each pile-up is

$$N = \int_0^{s/2} n(x) \, \mathrm{d}x = \frac{\bar{\tau} - \tau_{\mathrm{c}}}{\pi A} \frac{s}{2}. \tag{33}$$

The displacement of material above the slip plane with respect to that below is given by

$$u_x(x, y) = bH(y) \int_x^{s/2} n(x') \, \mathrm{d}x', \tag{34}$$

where H is the Heaviside function and the pile-ups are assumed to lie at $y = 0$ in the volume considered here. Differentiating the previous equation with respect to y yields

$$\partial_y u_x(x, y) = b\delta(y) \int_x^{s/2} n(x') \, \mathrm{d}x'. \tag{35}$$

with δ the Dirac distribution. The corresponding amount of plastic slip is defined by

$$\begin{aligned} \gamma^{\mathrm{p}}(x) &= \frac{1}{l} \int_{-l/2}^{l/2} \partial_y u_x(x, y) \, \mathrm{d}y \\ &= \frac{b}{l} \int_x^{s/2} n(x') \, \mathrm{d}x' \qquad (36) \\ &= \frac{b}{l} \frac{\bar{\tau} - \tau_{\mathrm{c}}}{\pi A} \left[\left(\frac{s}{2} \right)^2 - x^2 \right]^{1/2} \quad \text{for} \quad -\frac{s}{2} \leqslant x \leqslant \frac{s}{2}. \qquad (37) \end{aligned}$$

It is assumed that the pile-ups are periodically distributed along direction y perpendicular to slip plane with period l. The length l is assumed to be large enough for the interaction between parallel pile-ups to be neglected. As a result, the distribution of

plastic slip in the channel is the arc of an ellipse. It vanishes at the tips of the pile-ups and takes its maximal value Nb/l at the centre. This distribution is therefore different from the parabolic profile found in § 2.2. The mean value of the plastic slip is

$$\bar{\gamma}^{\mathrm{p}} = \frac{2}{s}\int_0^{s/2} \gamma^{\mathrm{p}}(x)\,\mathrm{d}x = \frac{b}{l}\frac{\bar{\tau}-\tau_{\mathrm{c}}}{4A}\frac{s}{2}. \tag{38}$$

It can be shown that the dislocation stress τ_{d} introduced in equation (30) does not depend on x, as required by the equilibrium condition

$$\tau_{\mathrm{d}} = -(\bar{\tau}-\tau_{\mathrm{c}}) = -\frac{2\mu l}{\pi(1-\nu)s}\,\bar{\gamma}^{\mathrm{p}}. \tag{39}$$

This proves that the double-ended dislocation pile-up produces a hardening component of linear kinematic type:

$$X = -\tau_{\mathrm{d}} = C\bar{\gamma}^{\mathrm{p}},$$

with

$$C = \frac{2\mu l}{\pi(1-\nu)s}. \tag{40}$$

We note that the pile-up model is formulated at a different level of approximation from the line-tension models of §§ 2.1 and 2.2. In particular, a periodic distribution of pile-ups is assumed along the y direction. This enables a dislocation stress τ_{d} to be present in the 1D model. Furthermore, each pile-up is completely embedded in an elastic matrix, so that the stress cannot relax. If the pile-ups were distributed continuously along the y direction, as the bowed dislocations in the previous sections are, the stress would then relax exactly as in § 2.2 and the local internal stresses and thus the macroscopic hardening would disappear.

§ 3. Cosserat model

The two-phase material now is a heterogeneous Cosserat continuum (see appendix A for the presentation of the Cosserat continuum). In § 3.1, both phases will be assumed to have a linearized behaviour, with different moduli. In §§ 3.2 and 3.3, the soft phase exhibits elastoplastic behaviour. In contrast with § 2.1 and similarly to § 2.2, we look here for solutions fulfilling all compatibility and equilibrium requirements with the only constraint that all fields must be periodic along x with period $s+h$ (see figure 1).

3.1. *Linear approximation*

Both phases are Cosserat linear materials with constants $\mu_h, \mu_{\mathrm{c}h}, \beta_h$ and $\mu_s, \mu_{\mathrm{c}s}, \beta_s$ (see appendix A for the definition of isotropic Cosserat elasticity). The moduli of phase s can also be treated as secant elastoplastic moduli and the elastic and plastic parts will not be distinguished. Phase h must be thought of as almost classical, which means that β_h is small, but the solution is given here in the general case.

A mean shear deformation $\bar{\gamma}$ is applied along the direction x. We look again for a displacement field of the form

$$u_x = \bar{\gamma}y, \quad u_y(x), \quad u_z = 0. \tag{41}$$

The deformation of a Cosserat material is described also by the microrotation axial vector field:

$$\phi_x = \phi_y = 0, \quad \phi_z = \phi(x). \tag{42}$$

Thus, the Cosserat deformation and curvature tensors (equations (A 1) and (A 2)) take the forms

$$\mathbf{e} = \begin{bmatrix} 0 & \bar{\gamma} + \phi & 0 \\ \partial_x u_y - \phi & 0 & 0 \\ 0 & 0 & 0 \end{bmatrix}, \quad \boldsymbol{\kappa} = \begin{bmatrix} 0 & 0 & 0 \\ 0 & 0 & 0 \\ \partial_x \phi & 0 & 0 \end{bmatrix}. \tag{43}$$

The associated non-vanishing components of the force and couple-stress tensors are

$$\sigma_{xy} = \mu(\bar{\gamma} + \phi + e_{yx}) + \mu_c(\bar{\gamma} + \phi - e_{yx}), \tag{44}$$

$$\sigma_{yx} = \mu(\bar{\gamma} + \phi + e_{yx}) - \mu_c(\bar{\gamma} + \phi - e_{yx}), \tag{45}$$

$$m_{zx} = 2\beta\, \partial_x \phi. \tag{46}$$

The balance equations give

$$\partial_x \sigma_{yx} = 0, \tag{47 a}$$

$$\partial_x m_{zx} - (\sigma_{xy} - \sigma_{yx}) = 0. \tag{47 b}$$

Taking the elasticity relations into account, these equations become

$$\mu(\partial_x \phi + \partial_x e_{yx}) - \mu_c(\partial_x \phi - \partial_x e_{yx}) = 0 \tag{48}$$

$$\beta\, \partial_{xx} \phi - \mu_c(\bar{\gamma} + \phi - e_{yx}) = 0. \tag{49}$$

Equation (48) can be rearranged to give

$$\partial_x e_{yx} = -\frac{\mu - \mu_c}{\mu + \mu_c}\, \partial_x \phi. \tag{50}$$

The equation for ϕ follows then from equation (49):

$$\beta\, \partial_{xxx} \phi - \frac{2\mu\mu_c}{\mu + \mu_c}\, \partial_x \phi = 0. \tag{51}$$

We define for each phase

$$\omega_s^2 = \frac{2\mu_s \mu_{cs}}{\beta_s(\mu_s + \mu_{cs})}, \quad \omega_h^2 = \frac{2\mu_h \mu_{ch}}{\beta_h(\mu_h + \mu_{ch})}. \tag{52}$$

Each ω is the inverse of a length. The solution of equation (51) takes the form

$$\phi_s = a_s \cosh(\omega_s x) + d_s \qquad \text{for} \quad -\frac{s}{2} < x < \frac{s}{2}, \tag{53}$$

$$\phi_h^+ = a_h \cosh\left[\omega_h\left(x - \frac{s+h}{2}\right)\right] + d_h \quad \text{for} \quad \frac{s}{2} < x < \frac{s+h}{2}, \tag{54}$$

$$\phi_h^- = a_h \cosh\left[\omega_h\left(x + \frac{s+h}{2}\right)\right] + d_h \quad \text{for} \quad -\frac{(s+h)}{2} < x < -\frac{s}{2}. \tag{55}$$

To reduce the number of integration constants in equations (53)–(55), the periodicity of ϕ has been used, together with the following symmetry conditions:

$$\partial_x \phi(0) = \partial_x \phi\left(-\frac{s+h}{2}\right) = \partial_x \phi\left(\frac{s+h}{2}\right) = 0. \tag{56}$$

Then, e_{yx} can now be determined from equation (50) as follows:

$$e^{s}_{yx} = -\frac{\mu_s - \mu_{cs}}{\mu_s + \mu_{cs}}\,\phi_s + e_s,$$

$$e^{h+}_{yx} = -\frac{\mu_h - \mu_{ch}}{\mu_h + \mu_{ch}}\,\phi^{+}_{h} + e_h, \tag{57}$$

$$e^{h-}_{yx} = -\frac{\mu_h - \mu_{ch}}{\mu_h + \mu_{ch}}\,\phi^{-}_{h} + e_h, \tag{58}$$

where e_h and e_s are integration constants. Furthermore, equation (49) implies that

$$e_{yx} = -\frac{\beta}{\mu_c}\,\partial_{xx}\phi + \bar{\gamma} + \phi, \tag{59}$$

$$\begin{aligned} e_{yx}(0) &= -\frac{\beta_s}{\mu_{cs}}\,a_s\omega_s^2 + \bar{\gamma} + a_s + d_s \\ &= -\frac{\mu_s - \mu_{cs}}{\mu_s + \mu_{cs}}\,(a_s + d_s) + e_s, \end{aligned} \tag{60}$$

$$\begin{aligned} e_{yx}\left(\frac{s+h}{2}\right) &= -\frac{\beta_h}{\mu_{ch}}\,a_h\omega_h^2 + \bar{\gamma} + a_h + d_h \\ &= -\frac{\mu_h - \mu_{ch}}{\mu_h + \mu_{ch}}\,(a_h + d_h) + e_h, \end{aligned} \tag{61}$$

from which the values of e_s and e_h are deduced:

$$e_s = \bar{\gamma} + d_s\,\frac{2\mu_s}{\mu_s + \mu_{cs}}, \quad e_h = \bar{\gamma} + d_h\,\frac{2\mu_h}{\mu_h + \mu_{ch}}. \tag{62}$$

For the determination of the four integration constants a_s, d_s, a_h and d_h, certain conditions at the interface must be enforced. In the Cosserat theory, the degrees of freedom, u_i and ϕ_i, are continuous if one excludes cracks and kinks. Therefore, the corresponding traction and couple-stress vectors must also be transmitted at the interface. Alternative conditions would be to prescribe specific values or jumps for displacement and microrotation at the interface, as done for instance by Shu and Fleck (1999). We note that in the dislocation-based model, the value of the step in lattice rotation given by equation (29), follows from the condition of mean prescribed glide $\bar{\gamma}$. Here, this condition is automatically satisfied by the periodicity requirement to be enforced by equation (67) below. Thus, continuity requirements are imposed in this work in the absence of a more specific interface model. The interface conditions require the following.

(i) Continuity of ϕ at $s/2$ is given by

$$a_s \cosh\left(\omega_s\,\frac{s}{2}\right) + d_s = a_h \cosh\left(\omega_h\,\frac{h}{2}\right) + d_h. \tag{63}$$

(ii) Continuity of m_{zx} at $s/2$ is given by

$$\beta_s a_s \omega_s \sinh\left(\omega_s\,\frac{s}{2}\right) = -\beta_h a_h \omega_h \sinh\left(\omega_h\,\frac{h}{2}\right). \tag{64}$$

(iii) Continuity of σ_{yx} at $s/2$ is obtained as follows. Rearranging equation (45) to give

$$\sigma_{yx} = (\mu + \mu_c)e_{yx} + (\mu - \mu_c)(\bar{\gamma} + \phi) = 2\mu(\bar{\gamma} + d) \tag{65}$$

one obtains the third equation

$$\mu_s(\bar{\gamma} + d_s) = \mu_h(\bar{\gamma} + d_h). \tag{66}$$

(iv) Periodicity of u_y implies that

$$\langle e_{yx} \rangle = \langle \partial_x u_y - \phi \rangle = \langle -\phi \rangle,$$

where the angular brackets denote averaging over x from $-(s+h)/2$ to $(s+h)/2$. One finds that

$$\langle \phi + e_{yx} \rangle = \left\langle \frac{2\mu_c}{\mu + \mu_c}\, \phi + e \right\rangle$$
$$= \left\langle \frac{2\mu_c}{\mu + \mu_c}\, \phi + \bar{\gamma} + \frac{2\mu}{\mu + \mu_c}\, d \right\rangle,$$

which gives the fourth equation

$$\frac{4\mu_{cs}}{\mu_s + \mu_{cs}} \frac{a_s}{\omega_s} \sinh\left(\omega_s \frac{s}{2}\right) + \frac{4\mu_{ch}}{\mu_h + \mu_{ch}} \frac{a_h}{\omega_h} \sinh\left(\omega_h \frac{h}{2}\right)$$
$$+ \bar{\gamma}(s+h) + 2d_s s + 2d_2 h = 0. \tag{67}$$

The four equations (63), (64), (66) and (67) represent a linear system of equations for the unknowns a_s, a_h, d_s and d_h. For conciseness, the final expressions are not given explicitly. Instead, the profiles of ϕ are plotted in figure 3 for two different

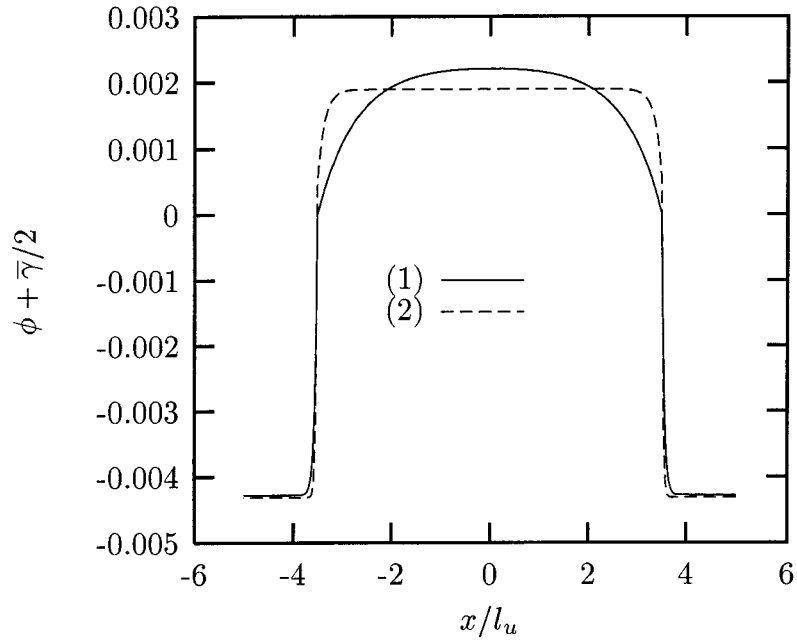

Figure 3. Distribution of microrotation of a two-phase linear elastic Cosserat material undergoing simple glide, using two different sets of parameters: (1) $\mu_h = 10\mu_s = 26\,923$ MPa, $\mu_{ch} = 20\mu_{cs} = 100\,000$ MPa and $\beta_h = \beta_s/30 = 100$ MPa l_u^2; (2) $\mu_h = 10\mu_s = 26\,923$ MPa, $\mu_{ch} = 20\mu_{cs} = 100\,000$ MPa and $\beta_h = \beta_s/100 = 1$ MPa l_u^2. l_u is the chosen length unit (mm, μm, etc.), $s + h = 10l_u$ and $\bar{\gamma} = 0.01$.

sets of material parameters. It can be seen that, for an appropriate choice of the material parameters ($\mu_h > \mu_s, \mu_{ch} > \mu_{cs}$ and $\beta_s > \beta_h$), ϕ_h is almost constant and ϕ_s displays a cosh profile with a characteristic length $1/\omega_s$. This profile mimics the distribution found in § 2.1 and suggests that ϕ can be interpreted as a lattice rotation, provided that ω_s is taken to be of the order of the magnitude of λ. A similar Cosserat elasticity model has been interpreted by Sedláček and Forest (2000) as a representation of anelasticity observed in crystals. Figure 3 has to be compared with figure 2 of the paper by Sedláček and Forest (2000) showing the bowing of screw dislocations in the channel.

In the limiting case when $\beta \to 0$, it can be shown that stresses and strains are constant in each phase, as expected for the solution of this simple glide problem for the classical Cauchy continuum. This can also be inferred from figure 3.

It can be checked also that $\langle \sigma_{yx} - \sigma_{xy} \rangle = 0$, so that the macroscopic stress is of course symmetric. This point indicates that we are implicitly considering the problem of the homogenization of heterogeneous Cosserat media. This general problem has been tackled by Forest *et al.* (1999, 2001a). The definition of the effective stress is

$$\bar{\sigma}_{ij} = \langle \sigma_{ij} \rangle.$$

If neither mean curvature nor relative rotation is prescribed to the unit cell, the effective stress is symmetric.

3.2. *Elastoplastic case*

Deformation in the soft phase is now decomposed into its elastic and plastic parts and the Schmid law is used as the yield criterion. The threshold shear stress τ_c is taken as constant (thus no hardening is considered). In contrast, we still do not distinguish between elastic and plastic curvature and keep a linearized relation between couple-stresses and total curvature. In this case, the total deformation in the cell is split into elastic and plastic parts:

$$\mathbf{e} = \mathbf{e}^e + \mathbf{e}^p. \tag{68}$$

Only single slip is considered. The normal $\boldsymbol{\nu}$ to the slip plane is assumed to be parallel to the y direction (figure 1) and the slip direction $\mathbf{s}$ is parallel to x:

$$\mathbf{e}^p = \gamma^p \mathbf{s} \otimes \boldsymbol{\nu} = \begin{bmatrix} 0 & \gamma^p & 0 \\ 0 & 0 & 0 \\ 0 & 0 & 0 \end{bmatrix}, \quad \mathbf{e}^e = \begin{bmatrix} 0 & e^e_{xy} & 0 \\ e^e_{yx} & 0 & 0 \\ 0 & 0 & 0 \end{bmatrix},$$

so that $e^e_{yx} = e_{yx}$. The non-vanishing force stress components are

$$\sigma_{xy} = \mu_s(e^e_{xy} + e_{yx}) + \mu_{cs}(e^e_{xy} - e_{yx}), \tag{69}$$

$$\sigma_{yx} = \mu_s(e_{yx} + e^e_{xy}) + \mu_{cs}(e_{yx} - e^e_{xy}). \tag{70}$$

The driving force to activate plastic slip is taken as the projection τ of the symmetric part of the force stress tensor on the normal to the slip plane, and in the slip direction. Kröner (1956) suggested using the full asymmetric force stress in the computation of the resolved shear stress. This is not done here since the main Cosserat effects shown in this work do not come from the asymmetry of stress but rather from the presence of lattice curvature and the associated couple stresses. Additional effects associated with the asymmetric character of the stress tensor

have not yet been studied. Comments on the role of the skew-symmetric part of the force stress tensor are given in §3.3. The yield criterion therefore gives

$$\tau = \frac{\sigma_{xy} + \sigma_{yx}}{2} = \tau_c = \mu_s(e^e_{xy} + e_{yx}). \tag{71}$$

From the first balance equation, namely $\partial_x \sigma_{yx} = 0$, and equation (71), it can be seen that e_{yx} and e^e_{xy} are constant. The second balance equation is

$$\beta_s\, \partial_{xx}\phi - \mu_{cs}(e^e_{xy} - e_{yx}) = 0, \tag{72}$$

which gives

$$\partial_{xxx}\phi = 0. \tag{73}$$

Thus, ϕ displays a parabolic profile in the cell. The wall of width h in figure 1 is taken as an elastic Cosserat solid. The profile is the same as in § 3.1:

$$\phi_s = a_s x_1^2 + d_s \quad \text{for} \quad -\frac{s}{2} < x < \frac{s}{2}, \tag{74}$$

$$\phi_h = a_h \cosh\left[\omega_h\left(x - \frac{s+h}{2}\right)\right] + d_h \quad \text{for} \quad \frac{s}{2} < x < \frac{s+h}{2}, \tag{75}$$

where ω_h is still given by equation (52). To determine the integration constants, the following conditions must be accounted for.

(i) Continuity of ϕ at $x = s/2$ is given by

$$a_s \frac{s^2}{4} + d_s = a_h \cosh\left(\omega_h \frac{h}{2}\right) + d_h. \tag{76}$$

(ii) Continuity of μ_{zx} is given by

$$\beta_s a_s s = -\beta_h a_h \omega_h \sinh\left(\omega_h \frac{h}{2}\right). \tag{77}$$

(iii) Continuity of σ_{yx}; e_{yx}, e^e_{xy} and σ_{yx} are determined in each phase:

$$e_{yx} + e^e_{xy} = \frac{\tau_c}{\mu_s}, \qquad e^e_{xy} - e_{yx} = \frac{2\beta_s}{\mu_{cs}}\, a_s,$$
$$\sigma^s_{yx} = \tau_c - 2\beta_s a_s, \quad \sigma^h_{yx} = 2\mu_h(\bar{\gamma} + d_h),$$

so that

$$2\mu_h(\bar{\gamma} + d_h) = \tau_c - 2\beta_s a_s. \tag{78}$$

(iv) Periodicity of u_y is found as follows. We use again the property

$$\langle e_{yx}\rangle = \langle \partial_x u_y - \phi\rangle = \langle -\phi\rangle,$$

$$e^s_{yx} = \frac{\tau_c}{2\mu_s} - \frac{\beta_s}{\mu_{cs}}\, a_s, \quad e^h_{yx} = -\frac{\mu_h - \mu_{ch}}{\mu_h + \mu_{ch}}\,\phi_h + \bar{\gamma} + d_h\,\frac{2\mu_h}{\mu_h + \mu_{ch}}, \tag{79}$$

$$e^s_{yx} + \phi_s = \frac{\tau_c}{2\mu_s} - \frac{\beta_s}{\mu_{cs}}\, a_s + a_1 x_1^2 + d_1,$$

$$e^h_{yx} + \phi_h = \frac{2\mu_{ch}}{\mu_h + \mu_{ch}}\,\phi_h + \bar{\gamma} + \frac{2\mu_h}{\mu_h + \mu_{ch}}\, d_h \tag{80}$$

$$= \frac{2\mu_{ch}}{\mu_h + \mu_{ch}}\, a_h \cosh\left[\omega_h\left(x - \frac{s+h}{2}\right)\right] + \bar{\gamma} + 2d_h, \tag{81}$$

from which the last equation for the determination of the integration constants is deduced:

$$\left(\frac{\tau_c}{2\mu_s} - \frac{\beta_s}{\mu_{cs}}\, a_s + d_s\right)s + \frac{a_s s^3}{12} + 2d_h h + \bar{\gamma} h + \frac{4\mu_{ch}}{\mu + \mu_{ch}}\,\frac{a_h}{\omega_h}\sinh\left(\omega_h\,\frac{h}{2}\right) = 0. \tag{82}$$

The linear system (76), (77), (78) and (82) can be solved for the four unknowns a_s, d_s, a_h, and b_h, as in the previous section.

Once the microrotation $\phi(x)$ is known, the amount of plastic slip can be found from

$$\gamma^p = \bar{\gamma} + \phi - \frac{\tau_c}{2\mu_s} - \frac{\beta_s a_s}{\mu_{cs}}. \tag{83}$$

The resulting parabolic distribution of Cosserat microrotation and plastic strain are given in figure 4 for two different sets of parameters. Note that, for the classical limiting case when β_s tends to zero (and μ_c to infinity, see next section), the classical relation (21) is retrieved.

3.3. *Limiting case for constrained Cosserat single-crystal plasticity*

At this point, a precise discussion of the links between the Cosserat microrotation ϕ and the lattice rotation ϕ^e must be given. The previous analysis of two different situations has shown the similarity between the profiles of ϕ and ϕ^e, as deduced from the combination of classical continuum mechanics and equilibrium of a dislocation line (§ 2). In the continuum framework of classical crystal plasticity, in which dislocations are not considered individually, a clear definition of lattice rotation exists. For instance, in the specific case of the shear test, it is given by equation (11). Such continuum description of lattice rotation will now be compared with the Cosserat microrotation computed in § 3.2. By definition, the lattice rotation is related to the skew-symmetric part of the elastic distortion:

$$\mathbf{e}^e = \begin{bmatrix} 0 & \bar{\gamma} - \gamma^p + \phi & 0 \\ \partial_x u_y - \phi & 0 & 0 \\ 0 & 0 & 0 \end{bmatrix}, \tag{84}$$

the corresponding axial vector being $(0,\ 0,\ (\bar{\gamma} - \gamma^p - \partial_x u_y)/2 + \phi)^T$.

If the skew-symmetric part of the Cosserat elastic deformation tensor vanishes, the following relation is found:

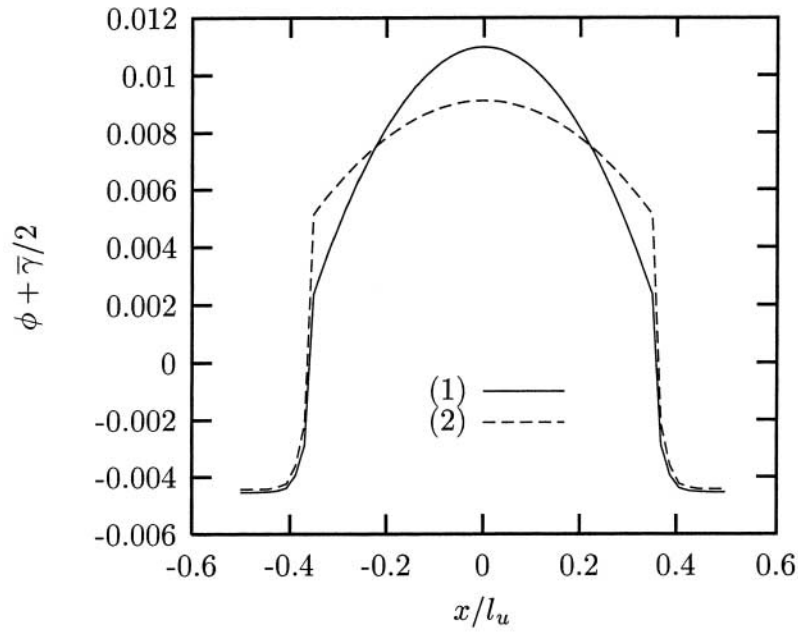

Figure 4. Distribution of microrotation of a two-phase elastoplastic Cosserat material undergoing simple glide, using two different sets of parameters: (1) $\mu_h = \mu_s = 26\,923$ MPa, $\mu_{ch} = 5\mu_{cs} = 500\,000$ MPa, $\beta_h = \beta_s/10 = 10$ MPa l_u^2 and $\tau_c = 10$ MPa; (2) $\mu_h = \mu_s = 26\,923$ MPa, $\mu_{ch} = s_{\mu_{cs}} = 500\,000$ MPa $\beta_h = \beta_s/30 = 1$ MPa l_u^2 and $\tau_c = 10$ MPa. $s + h = l_u$ and $\bar{\gamma} = 0.01$.

$$\phi = -\frac{\bar{\gamma} - \gamma^p - \partial_x u_y}{2}, \tag{85}$$

which is exactly that given by equation (11). Thus, the Cosserat microrotation is found to coincide exactly with the standard definition of lattice rotation when the Cosserat elastic deformation is symmetric. It is recalled that the skew-symmetric part of the stress and elastic deformation are linked by the elastic modulus μ_c (see equations (69) and (70)). Thus the value of μ_c controls the difference between the Cosserat microrotation and lattice rotation. The physical meaning of ϕ in the case of crystal plasticity is therefore clear only when it is close or equal to the lattice rotation. This is the case when μ_c is large compared with the other moduli. The condition $\mu_c \to \infty$ enforces indeed the symmetry condition for the elastic deformation. The resulting finite skew-symmetric part of the stress can be regarded as reaction stresses (similarly to pressure in classical incompressible materials). This is a kind of constrained Cosserat continuum for which the Cosserat microrotation follows strictly lattice rotation, which is different from the well-known couple-stress medium, for which the Cosserat rotation is forced to follow the material rotation, namely pure rotation component of the overall deformation gradient (Koiter 1963).

Consider the analysis of § 3.2 in the case when μ_c goes to infinity. The equations are indeed simplified and a clearer connection between material and geometric constants can be derived. The characteristic length in the hard phase becomes:

$$\frac{1}{\omega_h} = \left(\frac{\beta_h}{2\mu_h}\right)^{1/2}. \tag{86}$$

In the previous system of four equations (76), (77), (78) and (82), the fourth equation now becomes

$$\left(\frac{\tau_c}{2\mu_s}+d_s\right)s+\frac{a_s s^3}{12}+(2d_h+\gamma)h-\frac{2\beta_s}{\mu_h}\,a_s s=0. \tag{87}$$

The solution can then be given in a rather concise form, at least for a_s which characterizes the parabolic profile of the lattice rotation distribution:

$$a_s=-6\,\frac{\bar{\gamma}(s+h)-(\tau_c/2\mu_h)(s+2h+s\mu_h/\mu_s)}{s^3+(\beta_s/\mu_h)(18s+12h+3s^2\omega_h\coth(\omega_h h/2))}. \tag{88}$$

It can be seen that, contrary to the result of the analysis in the purely linear case of § 3.1, both material and geometric parameters contribute to the shape of the distribution ϕ in the elastoplastic channel. It can also be noted that, when $\beta_h\to 0$, that is $\omega_h\to\infty$, the coefficient a_s vanishes and the classical homogeneous distribution of rotation and plastic slip is retrieved. Interestingly, when a non-zero and constant value of β_h is assumed and when $\beta_s\to 0$, the coefficient a_s does not vanish but rather reaches the limit:

$$a_s=-6\left(\bar{\gamma}-\frac{\tau_c}{\mu}\right)\frac{s+h}{s^3}, \tag{89}$$

where $\mu_h=\mu_s=\mu$ has been assumed for simplicity. The fact that the classical homogeneous solution is not found in this case can be interpreted as follows. Letting β_s vanish in the moment of momentum balance equation (72) makes this second partial differential equation disappear, so that in principle we are left with the usual force stress balance equation and a classical solution could be expected. However, if equation (72) is multiplied by $1/\beta_s$ and differentiated again, we are left with equation (73) which can be assumed to hold in the limit for $\beta_s\to 0$. It amounts then to finding a parabolic distribution of ϕ fulfilling the classical equation (21) and continuity conditions at the interface. Indeed, for very low values of β_s, finite-element simulations provide this limit solution. Identifying the present result (89) and the corresponding solution of the dislocation model (6), the link between the Cosserat model and the intrinsic length scale is

$$\frac{1}{\lambda^2}=24\left(\frac{\bar{\gamma}\mu}{\tau_c}-1\right)\frac{s+h}{s}\approx\varrho_m, \tag{90}$$

which provides a reasonable but very approximate estimate of the density of mobile dislocations. The complete solution with all available material constants is of course more elaborate and incorporates the length scale associated with a non-vanishing β_s. In the latter case, the complete identification of the Cosserat model with the corresponding dislocation model can be made using equation (88) in order to calibrate β_s, as a function of ϱ_m.

§ 4. Comparison with strain-gradient plasticity models

Alternative non-local continuum theories are available to model size effects in crystal plasticity, usually called strain-gradient plasticity models. In this section, the response predicted by two of them is investigated in the simple case of shearing of laminate microstructures. In particular, the shape of the inhomogeneous plastic slip profiles are compared with the previous Cosserat results.

4.1. *Second gradient formulation*

Based on the continuum framework introduced by Mindlin and Eshel (1968) and Germain (1973), a strain-gradient plasticity constitutive framework has been developed by Fleck and Hutchinson (1997) and Shu and Fleck (1999). Two main models have been proposed by these workers. The first deals with isotropic plasticity, and the second with crystal plasticity. The main constitutive and balance equations are recalled in appendix B in a simplified case of single slip. Moreover, the originally viscoplastic framework is translated into a purely elastoplastic framework, for which analytical solutions can be found in the shear test considered in this work.

As in § 3, the displacement field in a periodic two-phase laminate microstructure subjected to mean shear deformation $\bar{\gamma}$ is considered. The solution must fulfil balance and constitutive equations in each phase and interface conditions. Firstly, a solution is obtained assuming a linear approximation for the constitutive behaviour without distinction between elastic and plastic parts. The second solution is valid for the nonlinear elastoplastic regime. These two solutions are to be compared with the results of §§ 3.1 and 3.2 respectively.

Using the same coordinate frame as in § 3, the solution still takes the form $u_x = (\bar{\gamma}y, u_y(x), 0)^{\mathrm{T}}$. The non-vanishing components of the strain-gradient tensor $\boldsymbol{\eta}$, as defined in appendix B, are

$$\eta_{xyx} = \eta_{yxx} = \tfrac{1}{2}\partial_{xx}u_y. \tag{91}$$

4.1.1. *Linear approximation*

Each phase is assumed to be a linear elastic second-grade continuum. The elastic laws link Cauchy stress to strain, and hyperstress to strain gradient:

$$\begin{aligned} \sigma_{xy} &= 2\mu\varepsilon_{xy} = \mu(\bar{\gamma} + \partial_x u_y), \\ m_{yxx} &= m_{xyx} = 2l_{\mathrm{e}}^2\mu\eta_{xyx} = \mu l_{\mathrm{e}}^2\,\partial_{xx}u_y. \end{aligned} \tag{92}$$

The equilibrium equation (B 3) reduces to

$$\partial_x\sigma_{xy} - \partial_{xx}m_{yxx} = 0. \tag{93}$$

The combination of the latter and the previous elastic relations leads to the following partial differential equation for u_y:

$$\partial_{xx}u_y - l_{\mathrm{e}}^2\,\partial_{xxxx}u_y = 0. \tag{94}$$

In the present linear approximation, lattice rotation cannot be distinguished from material rotation

$$\phi = \frac{\partial_x u_y - \bar{\gamma}}{2}, \tag{95}$$

so that ϕ obeys a similar partial differential equation:

$$\partial_x\phi - l_{\mathrm{e}}^2\,\partial_{xxx}\phi = 0, \tag{96}$$

which is identical to equation (51). In each phase the solution takes the form (53) with

$$\omega = \frac{1}{l_{\mathrm{e}}}. \tag{97}$$

The integration constants are determined from the interface and periodicity conditions. If no special behaviour is attributed to the interface, the pairs (u, t) and $(\mathrm{D}u, r)$, defined in appendix B, must be continuous:

(i) Continuity of displacement u_y and normal gradient of displacement is given by

$$\mathrm{D}u_y = \partial_x u_y = \bar{\gamma} + 2\phi. \tag{98}$$

This condition implies the continuity of ϕ which was also required in the Cosserat model.

(ii) Continuity of the traction vector is given by

$$t_x = (\sigma_{xy} - \partial_x m_{yxx}) n_x = 2\mu_i(\bar{\gamma} + \phi - l_{ei}^2 \partial_{xx}\phi) = 2\mu_i(\bar{\gamma} + d_i), \tag{99}$$

where the index $i = s, h$ stands for the label of the phase, and d_i is the constant term in the cosh solution, as in equation (53).

(iii) Continuity of the double-traction vector is given by

$$r_y = m_{yxx} n_x = 2\mu l_e^2 \, \partial_x \phi. \tag{100}$$

(iv) Periodicity of u_y is given by $\langle \partial_x u_y \rangle = 0$.

It can be seen that the interface conditions (98)–(100) are identical with the conditions (63)–(66) appearing in the Cosserat model. Thus the strain-gradient and the Cosserat models provide the same solution in the present simple situation.

4.1.2. *Elastoplastic case*

Adopting the additive decomposition (B 1) of total strain and strain gradient into elastic and plastic parts, the elastic laws become

$$\sigma_{xy} = 2\mu\varepsilon_{xy}^{\mathrm{e}} = \mu(\bar{\gamma} + u_{y,x} - \gamma^{\mathrm{p}}), \tag{101}$$

$$m_{yxx} = 2l_{\mathrm{e}}^2 \mu(\eta_{yxx} - \eta_{yxx}^{\mathrm{p}}) = l_{\mathrm{e}}^2 \mu(\partial_{xx} u_y - \gamma^{\mathrm{S}}), \tag{102}$$

where γ^{S} is the slip gradient variable (see appendix B). The yield condition is a generalized Schmid law involving resolved shear stress and hyperstress:

$$\sigma_{\mathrm{eq}} = |\tau| + \frac{|m|}{l_{\mathrm{p}}} = \sigma_{xy} + \frac{m_{yxx}}{l_{\mathrm{p}}} = \tau_{\mathrm{c}}. \tag{103}$$

It must be noted that a second characteristic length l_{p} enters the yield criterion. The yield condition combined with the unchanged balance equation (93) can then be shown to lead to the following partial differential equations:

$$\partial_{xx} u_y - l_{\mathrm{p}}^2 \, \partial_{xxxx} u_y = 0, \quad \partial_x \gamma^{\mathrm{p}} - l_{\mathrm{p}}^2 \, \partial_{xxx} \gamma^{\mathrm{p}} = 0. \tag{104}$$

Since the definition of lattice rotation (21) still holds, one is led to the following partial differential equation for ϕ:

$$\partial_x \phi - l_{\mathrm{p}}^2 \, \partial_{xxx} \phi = 0, \tag{105}$$

which again gives a cosh profile but associated with the characteristic length l_{p}. This result is different from the parabolic profile found in the same analysis with the Cosserat model. The reason is, however, clear: it stems from the modified yield condition (103). A consequence of this choice is that shear stress σ_{xy} does not remain

constant in space, contrary to all investigated cases in the previous sections. It introduces hardening associated with strain gradient.

The strain gradient model can, however, be slightly modified to be closer to the simple Cosserat constitutive equations used in § 3.2. We let l_p go to infinity and do not distinguish elastic and plastic parts in $\boldsymbol{\eta}$:

$$\sigma_\mathrm{eq} = \tau = \sigma_{xy} = \tau_\mathrm{c}, \quad m_{yxx} = 2\mu l_\mathrm{e}^2 \eta_{yxx}. \tag{106}$$

l_e is in fact here the characteristic length of the elastoplastic secant moduli in the second elasticity law, since $\boldsymbol{\eta}$ has not been partitioned. The balance equation (93) now yields:

$$\partial_{xxxx} u_y = 0, \quad \partial_{xxx} \gamma^\mathrm{p} = 0, \quad \partial_{xxx} \phi = 0, \tag{107}$$

and a parabolic profile is retrieved.

4.2. *Crystal plasticity with a gradient of internal variable*

One of the earliest proposals to introduce higher-order gradients in the relevant constitutive variables is the Aifantis model that belongs to a class of generalized continua different from the theories used in the previous sections. The models presented and illustrated by Aifantis (1987, 1999) do not introduce additional rotational degrees of freedom like the Cosserat theory, nor higher-order derivatives of the displacement field. Instead, the constitutive behaviour of the material is assumed to depend on an internal variable γ^p and its gradient grad γ^p. The free energy is a function of temperature, elastic strain, plastic slip and its gradient. The classical expression of work of internal forces is in fact complemented by terms related to the internal variable and its gradient (Huang *et al*. 2001):

$$p^\mathrm{int} = \sigma_{ij} \dot{\varepsilon}_{ij} + \alpha \dot{\gamma}^\mathrm{p} + B_i \, \partial_i \dot{\gamma}^\mathrm{p}, \tag{108}$$

where α and B_i are the thermodynamic forces associated with the internal variable and its gradient. The principle of virtual work can be used to derive the balance equations:

$$\operatorname{div} \boldsymbol{\sigma} = 0, \quad \alpha = \operatorname{div} \mathbf{B}. \tag{109}$$

The classical balance equation is conserved, whereas the second equation can be regarded as a definition of the introduced generalized force α. The degrees of freedom and associated reaction forces are therefore the pairs $(u_i, t_i = \sigma_{ij} n_j)$ and $(\gamma^\mathrm{p}, B = B_i n_i)$. The dissipation rate takes the form

$$D = \sigma_{ij} \dot{\varepsilon}_{ij}^\mathrm{p} + (\operatorname{div} \mathbf{B}) \dot{\gamma}^\mathrm{p} = (\tau + \operatorname{div} \mathbf{B}) \dot{\gamma}^\mathrm{p}. \tag{110}$$

The latter expression leads one to propose a yield condition of the form

$$\sigma_\mathrm{eq} = \tau + \operatorname{div} \mathbf{B} = \tau_\mathrm{c}. \tag{111}$$

In the Aifantis model, $\mathbf{B}$ is assumed to be simply proportional to grad γ^p (quadratic potential):

$$B_i = c \, \partial_i \gamma^\mathrm{p}, \tag{112}$$

where c is a constitutive parameter. The yield condition (111) then becomes

$$\tau = \tau_\mathrm{c} - c \, \nabla^2 \gamma^\mathrm{p}, \tag{113}$$

which is the well-known gradient-enhanced yield criterion, with ∇^2 being the Laplace operator.

This theory is now applied to the simple situation investigated in the present article. The yield condition reduces to the simple form

$$\tau = \sigma_{xy} = \tau_c - c\,\partial_{xx}\gamma^p. \tag{114}$$

The equilibrium equation requires constant shear stress so that we must have

$$\partial_{xxx}\gamma^p = 0. \tag{115}$$

The elasticity relation (101) implies again that $\partial_{xx}u_y = \partial_x\gamma^p$ so that lattice rotation ϕ must fulfil the same partial differential equation:

$$\phi = \frac{\partial_x u_y + \gamma^p - \bar{\gamma}}{2}, \quad \partial_{xxx}\phi = 0. \tag{116}$$

This model therefore gives the same answer for the lattice rotation and plastic slip distribution as the Cosserat model of § 3.2, namely a parabolic distribution. The interface conditions are dictated by the chosen degrees of freedom and associated forces.

(i) The displacement u_y and traction vector $\sigma_{xy}n_x$ are continuous across the interface.
(ii) Plastic slip γ^p and force $B = (c\,\mathrm{grad}\,\gamma^p)n = c\,\partial_x\gamma^p$ are continuous across the interface.

In contrast with the Cosserat theory, plastic slip is assumed to be continuous, whereas lattice rotation need not necessarily be continuous (this comes from the fact that $\partial_x u_y$ is not necessarily continuous in contrast with the strain-gradient theory).

If linear hardening is introduced in the yield condition (111), it can be shown that a cosh distribution is obtained. However, this situation cannot be compared with that of §§ 2 and 3 since no hardening was taken into account there.

§ 5. Discussion

5.1. *Direct comparison between the dislocation and generalized-continuum frameworks*

A direct comparison between the dislocation models and the continuum frameworks is difficult insofar as the dislocation models considered in this work are very specific whereas the continuum models can be used in very general situations. The line-tension model considers a representative bowing screw dislocation which is a convenient and idealized situation. As for the pile-up model, it deals with periodic arrays of edge dislocations. However, a parallel between the line-tension dislocation model and the Cosserat, the second gradient and the Aifantis models can be drawn, as shown in table 1. All models share the main variables plastic slip γ^p and lattice rotation ϕ^e, even though the two gradient models more explicitely introduce the gradient of plastic slip. The classical divergence equation for the stress tensor is valid for all the theories. The generalized continuum involves an additional (or a higher order) balance equation which reflects in a continuum way the dislocation line tension equilibrium equation. A one-to-one identification is not possible, however, since the continuum theories do not explicitly introduce densities of line defects. The consequence is that the governing partial differential equations in the case of shear-

Table 1. Comparison between the line-tension dislocation model and three generalized-continuum frameworks with application to the periodic simple glide of a two-phase laminate microstructure in elastoplasticity: balance and constitutive equations, interface conditions and characteristic lengths. The governing partial differential equations are given only in the case of an elastoplastic soft phase.

	Main variables	Balance equations	Governing partial differential equation for simple glide	Constitutive equations	Continuity at interface	Characteristic length
Dislocation model	$\varphi/\gamma^{\mathrm{p}}$	$\operatorname{div}\boldsymbol{\sigma}=0$	$\lambda^2\,\partial_{xx}\gamma^{\mathrm{p}}=-\dfrac{\bar{\tau}}{\mu}$	$\sigma_{xy}=2\mu\varepsilon^{\mathrm{e}}_{xy}$	Neither γ^{p} nor ϕ	
	ϕ^{e}	$\tau b+T\,\partial_{xx}\varphi=0$	$\lambda^2\,\partial_{xx}\phi^{\mathrm{e}}_{\mathrm{s}}=-\dfrac{\bar{\tau}}{\mu}$	$\lvert\tau\rvert-\tau_{\mathrm{c}}\leqslant 0$	$\mathbf{t}$	$\left(\dfrac{T}{\mu\varrho_{\mathrm{m}}b^2}\right)^{1/2}$
Cosserat model	γ^{p}	$\operatorname{div}\boldsymbol{\sigma}=0$	$\beta_s\,\partial_{xx}\gamma^{\mathrm{p}}-\mu_{\mathrm{cs}}(e^{\mathrm{e}}_{xy}-e_{yx})=0$	$\sigma_{xy}=(\mu+\mu_{\mathrm{c}})\varepsilon^{\mathrm{e}}_{xy}+(\mu-\mu_{\mathrm{c}})\varepsilon^{\mathrm{e}}_{yx}$	ϕ	$\left(\dfrac{\beta_s}{\mu_{\mathrm{cs}}}\right)^{1/2}$ or $\left(\dfrac{1}{a_s}\right)^{1/2}$
	ϕ	$\operatorname{div}\boldsymbol{\mu}-\boldsymbol{\epsilon}:\boldsymbol{\sigma}=0$	$\beta_s\,\partial_{xx}\phi-\mu_{\mathrm{cs}}(e^{\mathrm{e}}_{xy}-e_{yx})=0$	$\sigma_{yx}=(\mu+\mu_{\mathrm{c}})\varepsilon^{\mathrm{e}}_{yx}+(\mu-\mu_{\mathrm{c}})\varepsilon^{\mathrm{e}}_{xy}$	$\mathbf{t}$	
				$m_{zx}=2\beta\,\partial_x\phi$	$\mathbf{r}$	given by
				$\lvert\tau\rvert-\tau_{\mathrm{c}}\leqslant 0$		equation (88)
Second gradient	γ^{p}	$\operatorname{div}(\boldsymbol{\sigma}-\operatorname{div}\mathbf{m})=0$	$\partial_x\gamma^{\mathrm{p}}-l_{\mathrm{p}}^2\,\partial_{xxx}\gamma^{p}=0$	$\sigma_{xy}=2\mu\varepsilon^{\mathrm{e}}_{xy}$	$\mathrm{D}\mathbf{u}$	
	γ^{S}		$\partial_x\phi-l_{\mathrm{p}}^2\,\partial_{xxx}\phi=0$	$m_{xyz}=2l_{\mathrm{e}}^2\mu\eta^{\mathrm{e}}_{xyz}$	$\mathbf{t}$	l_{p}
				$\lvert\tau\rvert+\dfrac{\lvert m_{xyx}\rvert}{l_{\mathrm{p}}}-\tau_{\mathrm{c}}\leqslant 0$	$\mathbf{r}$	
Gradient of	γ^{p}	$\operatorname{div}\boldsymbol{\sigma}=0$	$c\,\partial_{xx}\gamma^{\mathrm{p}}+\bar{\tau}-\tau_{\mathrm{c}}=0$	$\sigma_{xy}=2\mu\varepsilon^{\mathrm{e}}_{xy}$	γ^{p}	
internal variable	$\partial_x\gamma^{\mathrm{p}}$	$\operatorname{div}\mathbf{B}=\alpha$	$c\,\partial_{xx}\phi+\bar{\tau}-\tau_{\mathrm{c}}=0$	$B_x=c\,\partial_x\gamma^{\mathrm{p}}$	$\mathbf{t}$	$\left(\dfrac{c}{\tau_{\mathrm{c}}}\right)^{1/2}$
				$\lvert\tau+c\,\Delta\gamma^{\mathrm{p}}\rvert-\tau_{\mathrm{c}}\leqslant 0$	B	

ing of the elastoplastic laminate microstructure have almost the same structure. The gradient theories are somewhat different, in the sense that they predict that the shear stress τ does not remain equal to the critical resolved shear stress τ_c. In the strain-gradient theory, the shear stress τ is equal to $\tau_c - m_{yxx}/l_p$ and to $\tau_c - c\,\partial_{xx}\gamma^p$ in the Aifantis model. This strain-gradient-induced hardening behaviour is not introduced nor predicted in the idealized line tension dislocation and Cosserat models. The strain-gradient theory can be simplified to eliminate this hardening component, as shown at the end of § 4.1.2. The similarity of the governing partial differential equation makes it possible to identify some parameters of the generalized-continuum models with the dislocation-based quantities, especially the characteristic lengths involved. These relations between the phenomenological moduli and the dislocation material parameters are gathered in the last row of table 1 and reveal the physical meaning of the moduli.

As a consequence of the choice of the primary variables, the interface conditions are different for all generalized-continuum models. In the line-tension model, at least in the plastic regime, plastic slip and lattice rotation are not necessarily continuous, which corresponds to a density of edge dislocations deposited at the interface. In contrast, the Cosserat theory assumes the continuity of lattice rotation whereas plastic slip is continuous in the gradient of internal variable theory. The second gradient model introduces the continuity of the normal gradient of displacement, the physical meaning of which is more difficult to assess. These differences in interface conditions make the previous identification of characteristic lengths at the level of the governing equations insufficient. That is why we must also compare the final solution, namely the predicted distribution of slip and lattice rotation in the considered simple glide test. As shown in § 3.3, the lattice distributions predicted by the Cosserat and the line-tension models can be identified. The phenomenological moduli are then related to dislocation material parameters but also to the geometry of the microstructure, especially the layer thicknesses s and h. This explains why two identifications of characteristic lengths are proposed for the Cosserat model in table 1: one for the direct comparison of the governing partial differential equations, and the other for the final explicit solutions taking the interface conditions into account. The same distinction could be made for the second gradient model in the elastoplastic regime without hardening.

This identification procedure is limited to the present idealized situation and does not ensure that the generalized-continuum theories will still be relevant under more general loading conditions.

5.2. *Inhomogeneous plastic deformation in channels*

In the simple situation investigated in this work, several available non-local models of crystal plasticity (ranging from the Cosserat, the second-grade to the gradient of internal variable theories) predict development of an inhomogeneous distribution of plastic slip and lattice rotation in the soft channels of the laminate microstructure under shear. Each of the non-local models has its own advantages and drawbacks. The Cosserat model naturally arises from almost 30-year-old theoretical reflections on crystal plasticity (Mandel 1973) but the physical meaning of the skew-symmetric part of the stress still remains unclear. In the strain-gradient model recalled in appendix B, the constitutive links between slip gradient variables γ^S and the gradient of slip, $\operatorname{grad}\gamma^p$, remains phenomenological. This model also gives the opportunity of incorporating effects that are not associated with geome-

trically necessary dislocations (in particular the gradient of slip in the direction normal to the slip plane, the physical interpretation of which remains to be explained). Regarding the Aifantis model, the Laplace term in yield condition (113) can in some cases be derived from the physics of dislocations (see for instance the paper by Estrin *et al*. (1998) in the case of double slip).

Anyway, the use of the Cosserat, the strain-gradient or the Aifantis models invariably leads to parabolic or cosh distributions of plastic slip and lattice rotation, depending on specific constitutive assumptions. Each profile is characterized by a length that is directly related to the constitutive length(s) introduced in each model. This intrinsic length enters the elastic or the plastic part of the constitutive equations, or both. Figure 5 summarizes and illustrates the different deformed states of a sample of such two-phase material, according to the classical and Cosserat models.

The parabolic or cosh distributions of plastic slip and lattice rotation result also from the line-tension dislocation-based model that incorporates the bowing of screw dislocations in narrow channels into a simple one-dimensional continuum-mechanics description. Loosely speaking, the anelastic regime for which dislocations move over short distances can be associated with a cosh distribution, whereas the fully plastic regime corresponds to a parabolic profile.

Thus it appears that the plastic slip and lattice rotation distribution obtained within the proposed Cosserat framework accurately mimics the results of the dislocation-based line tension models. On the generalized-continuum level, simple linear and/or perfectly plastic constitutive equations that are usual in

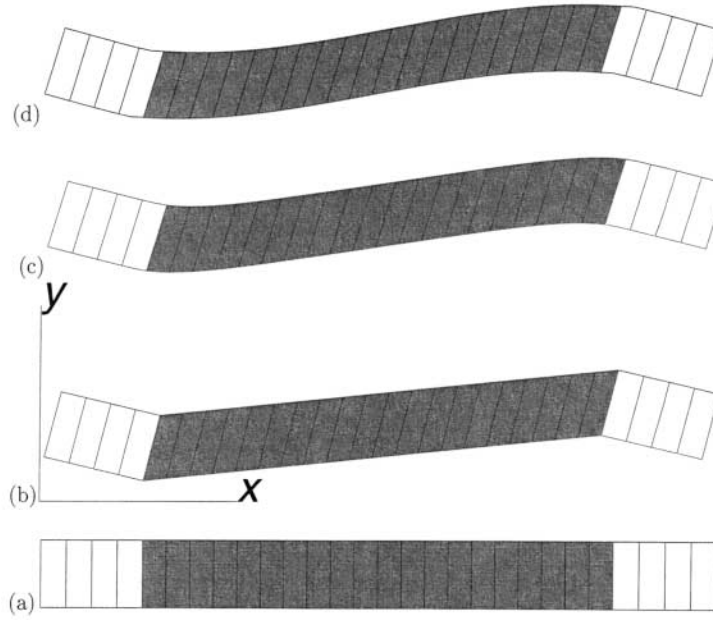

Figure 5. Deformed states of a two-phase material element under simple shear: (*a*) initial state; (*b*) solution according to classical crystal plasticity; (*c*) Cosserat elasticity (see § 3.1); (*d*) Cosserat elastoplasticity (see § 3.2). The solutions have been computed using the finite-element method and each phase is divided into elements; the hard phase shown in white, and the soft phase in grey; the mean deformations are the same in (*b*)–(*d*).

phenomenological modelling can be used. The balance of moment of momentum equation (47*b*), which does not exist in the classical continuum framework, turns out to be the continuum counterpart of the equilibrium condition (1) for a representative dislocation bowing in the channel.

Even a direct identification of the dislocation and Cosserat models is possible. In particular, the wavelength λ of the dislocation model (6) enables one to compute the corresponding value of the Cosserat parameter β_s from equation (86):

$$\beta_s \approx \frac{2\mu}{\varrho_{\mathrm{m}}}. \tag{117}$$

Since it depends on the density of mobile dislocations which may vary during deformation, β_s should not be seen as a constant material parameter. In the case of the parabolic profile, not only the constant β_s but also explicitly the channel width s are the determinant parameters (see equation (89)). The identification for the isostrain model has been proposed by Sedláček and Forest (2000). The present work focuses on the detailed solution of the isostress periodic problem. Other models such as the strain-gradient and the Aifantis models have been shown to reproduce the line-tension effects as well.

Interestingly, the above-mentioned non-local theories were not originally designed for the modelling of line-tension effects but rather hardening effects due to so-called geometrically necessary dislocations as in the pile-up model. Admittedly, several nonlocal models have shown their ability to account for particle or grain-size effects that can be related to the presence of dislocation pile-ups (see the papers by Acharya and Beaudoin (2000) and Forest *et al.* (2000) for the simulation of Hall–Petch effects in polycrystals). However, one should not hastily associate strain-gradient plasticity and dislocation pile-up effects. In fact, the distribution of plastic slip in dislocation pile-ups in the soft phase is not correctly described by any of the above-mentioned non-local models. Double-ended pile-ups are dislocation structures that can also form in the laminate microstructure under the prescribed loading conditions, for instance because of periodically distributed Frank–Read sources, or as the result of passage of many bowed screw dislocations. It could be argued that the pile-up model includes internal stresses and associated hardening, which has not been taken into account in the Cosserat model. However, the strain-gradient model used in § 4.1 incorporates hardening associated with hyperstresses and still provides a cosh distribution. A Cosserat model including classical linear hardening would lead in fact also to a cosh distribution. It is thought that one of the main contributions of this paper is indeed that it shows that the main ingredients of the current non-local crystal plasticity models are not really best suited to the description of dislocation pile-up effects in crystals, but rather of dislocation line-tension effects. This is surprising since the size effects arising from dislocation bowing did not belong explicitly to the initial main motivations that have led to the development of the non-local theories. Conversely, this fact can be regarded as an important property of the non-local models since the line-tension effects have proved to dominate the mechanical response of many engineering materials. The case of single-crystal nickel-based superalloys is of special interest, since they display a periodic microstructure of hard precipitates and soft channels. A description of precipitate size effects in single-crystal superalloys based on the Cosserat theory can be found in the paper by Forest *et al.* (2000). An alternative model including gradients of internal variables has also been applied to this single-crystal material (Busso *et al.* 2000). Size effects

associated with the channel width are predicted by the models. For example, it can be checked that the solution of the elastoplastic Cosserat model tends towards the classical model when the relative size s/h goes to infinity (the coefficient a_s of the parabolic profile then vanishes according to equation (88)).

The presented results are applicable to cyclic loading conditions. Further effort must now be concentrated on dislocation interaction and hardening, which remains challenging since the line tension model becomes difficult to handle explicitly in the 3D case (Sedláček *et al.* 2003). Dislocation dynamics and finite-element simulations are then useful tools to go towards more realistic multiple-slip situations, as initiated by Shu and Fleck (1999) and Shu *et al.* (2001). The situation of double slip has been shown to be dramatically different from the single-slip case by Shu *et al.* (2001), from the dislocation dynamics point of view.

5.3. *Role of interface conditions*

In the present study, non-local mechanical models incorporating additional higher-order boundary or interface conditions have been considered. It appears clearly in the work of Shu *et al.* (2001) that models that keep the classical structure of the boundary value problem unchanged, such as those of Acharya and Bassani (2000) and Busso *et al.* (2000), predict homogeneous glide as the classical continuum mechanics does for the shearing of a crystalline layer. Inhomogeneous distributions can be obtained with a non-local model by applying higher-order boundary conditions at the boundary of the sheared layer. The higher-order boundary conditions concern the additional degrees of freedom of higher-order derivatives, introduced in the model, and their associated forces. Similarly, in the two-phase microstructure considered in this work, the enriched interface conditions are responsible for the development of an inhomogeneous plastic slip pattern in the soft phase. Since neither special constitutive properties nor direct boundary conditions have been applied to the interface, both phases must be treated as generalized continua, and not only the soft phase. If one considers in the Cosserat model of § 3 the limit case for which $\mu_{ch} = \infty$ and $\beta_h = 0$, constant values for ϕ are obtained in each phase with a jump. This means that, in order to obtain a non-constant distribution, the wall cannot be regarded as purely classical; it must be able to carry the surface couples produced in phase s at the boundary. This can be achieved by setting a relatively low value of β_h and a 100 times larger β_s. In that case, the distribution in the hard phase is then almost flat with a steep rise close to the boundary, which mimics a jump of the considered variable. The same holds for the other two non-local models handled in § 4. An alternative method could be to consider the hard phase as a classical material and to set directly boundary conditions at the interface (see for instance the paper by Shu and Fleck (1999) for the interface between two crystallites). This has not been done here because the conditions to be prescribed are not necessarily known *a priori*. Instead, in the Cosserat theory, lattice rotation, the additional degree of freedom, is continuous at the interface and so are the traction vector and the couple-stress vector. Similarly in the second gradient theory, the normal gradient of the displacement and the associated force must be continuous at the interface, and so are plastic slip and associated force in the Aifantis model. These conditions are therefore slightly different for each theory, even if the governing partial differential equations are the same in the bulk. It is, however, difficult to assess which continuity requirement is the most realistic from the physical point of view. The main point is

that these continuity constraints are the origin of the non-uniform lattice rotation field in the soft phase.

5.4. *Description of internal stresses and hardening*

Attention has been focused on the continuum description of plastic slip and lattice rotation distribution, but the question of hardening is also an important point from the macroscopic point of view. The pile-up model of § 2.3 leads to the existence of linear hardening due to internal stresses, described by equation (40). This kinematic hardening component can be seen as a sort of non-local hardening law since it depends on the mean value of plastic slip and not on the local value of γ. It has the classical form used in phenomenological constitutive equations for a single crystal under cyclic loading (Méric *et al.* 1991), although nonlinear kinematic hardening is usually observed experimentally. It appears also that this hardening term does not depend on the lattice curvature or the dislocation density tensor and therefore has no direct relation to the density of geometrically necessary dislocations (see also Mughrabi (2001)). A size effect is expected from the dependence of the hardening modulus C on the channel width s (see equation (40)).

Such a hardening term should be introduced in the continuum model of § 3.2 to account for arising internal stresses. This can easily be done by replacing τ_c in equation (71) by a term of the form $\tau_c + C\bar{\gamma}$. The form of the solution is not affected by this term which does not depend on the position x. It is clear, however, that the continuum Cosserat model does not account for the exact distribution of plastic strain in a double-ended pile-up (parabolic profile instead of an elliptic profile). The introduction of the linear hardening component then keeps a phenomenological character.

Shu *et al.* (2001) identified numerically the local hardening modulus entering the constitutive equations of the second gradient model using the mean response of the discrete dislocation dynamics model. The hardening modulus links the equivalent stress and plastic strain rates $\dot{\sigma}_{eq}$ and $\dot{q}$ (see § 4.1). However, the plastic multiplier q is a measure of cumulated plastic strain and strain gradient without distinction, because of the use of a single coupled yield criterion (103) in the spirit of de Borst (1991):

$$\dot{q} = |\dot{\gamma}^p| + l_p|\dot{\gamma}^S|. \tag{118}$$

The pile-up model indicates that hardening originates from mean plastic slip and not from the local slip gradient. Accordingly, a distinction between both contributions should be preferable in the continuum model. Such a distinction exists in the full Cosserat model used by Forest *et al.* (2000) by considering two different plastic multipliers; one for plastic slip, and the other for lattice curvature. This means also that the single yield criterion (103) is replaced by two yield conditions: one involves resolved shear stresses, and the second involves resolved couple stresses. Coupling between both comes then from the hardening laws. It must be noticed that this hardening law for the two-phase material must be of kinematic type for application to cyclic plasticity.

§ 6. Conclusions

Bowing of dislocations possessing line tension has been incorporated in a simple 1D continuum model of plastic deformation of laminate microstructure and used to

calibrate non-local crystal plasticity continuum models. The 1D laminate can be considered to be a simple model of many real mesoscale microstructures: nickel-based superalloys, microlaminates, thin films, or dislocation substructures.

The dislocation-based as well as the generalized-continuum models lead to (size-dependent) inhomogeneous distribution of plastic slip and lattice rotation in the soft channels. This indicates that the non-local theories can be identified with an uncertainty range unless the physical meaning of the introduced variables and moduli are clearly specified. In particular, the present work shows the following.

(i) The non-local models may reflect the bowing of dislocations with line tension rather than the hardening due to storage of geometrically necessary dislocations.
(ii) The additional or higher-order balance equations introduced in the non-local models turn out to be the counterparts of the equilibrium equation for bowing dislocations.
(iii) The microrotation of the Cosserat model can be identified with the classical lattice rotation, provided that the Cosserat elastic deformation is symmetric.
(iv) The intrinsic length scale can be related to the density of the bowing dislocations; thus it is *no* constant material parameter.
(v) The higher-order interface conditions responsible for the inhomogeneous distribution of plastic slip and lattice rotation can be related to the requirement for continuity of lattice rotation for the Cosserat continuum, or of other higher-order quantities.

Finally we should like to stress that we are aware that there are many different sources of strain gradients in plasticity, on many different length scales. The present results apply to the situation considered in the paper, namely bowing of dislocations between narrowly spaced obstacles. General validity of the present results (i.e. the explicit relations between line-tension effects and the generalized-continuum description) for more realistic microstructures, more general loading conditions and/or multislip orientations is limited mainly by the fact that the (non-trivial) extension of the dislocation-based line-tension model in three dimensions is in an embryonic state (Sedláček *et al.* 2003).

The main advantage of the generalized-continuum plasticity models, compared with the proposed continuum dislocation-based model, is that they can be more easily extended to describe more general situations than simple shear under single slip. In fact, 3D versions of most generalized-continuum theories are available. Then, results obtained by, for example, finite-element computations should be compared with 3D dislocation dynamics simulations which correctly account for the line tension effects of curved dislocations (Kubin *et al.* 1992, Devincre *et al.* 2001).

APPENDIX A

The Cosserat continuum

The Cosserat continuum is described by a displacement field $\mathbf{u}$ and an independent rotation field called microrotation and represented by an axial vector $\boldsymbol{\phi}$. The Cosserat deformation tensor is

$$e_{ij} = \partial_{x_j} u_i + \epsilon_{ijk}\phi_k, \tag{A 1}$$

with ϵ_{ijk} being the sign of the permutation (i, j, k) of $(1, 2, 3)$. The curvature $\boldsymbol{\kappa}$ of the medium is related to the rotation field, as follows:

$$\kappa_{ij} = \partial_{x_j} \phi_i. \tag{A 2}$$

The stress tensors associated with the previous deformation and curvature are the force stress tensor $\boldsymbol{\sigma}$ and the couple-stress tensor $\mathbf{m}$ respectively. They must fulfil the balance of momentum and the balance of moment of momentum equations, namely:

$$\partial_{x_j}\sigma_{ij} = 0, \quad \partial_{x_j}\mu_{ij} - \epsilon_{ijk}\sigma_{jk} = 0, \tag{A 3}$$

where volume forces and couples are not considered for simplicity. The traction and couple stress vectors are given by

$$t_i = \sigma_{ij} n_j, \quad r_i = m_{ij} n_j, \tag{A 4}$$

where $\mathbf{n}$ is the unit normal to the boundary.

A boundary value problem is well-posed for the Cosserat continuum if boundary conditions are given to one element of each pair displacement–traction (u_i, t_i) and microrotation–couple-stress vector (ϕ_i, r_i) for all $i = 1, 3$.

The constitutive equations for isotropic Cosserat elasticity involve six elastic moduli, namely the two Lamé constants λ and μ and four additional moduli:

$$\sigma_{ij} = \lambda e_{kk}\,\delta_{ij} + 2\mu e_{(i,j)} + 2\mu_c e_{\{i,j\}}, \tag{A 5}$$

$$m_{ij} = \alpha\kappa_{kk}\,\delta_{ij} + 2\beta\kappa_{(i,j)} + 2\gamma\kappa_{\{i,j\}}, \tag{A 6}$$

where $e_{(i,j)}$ and $e_{\{i,j\}}$ denote the symmetric and skew-symmetric parts of $\mathbf{e}$ respectively. In the 2D case, the constant α in equation (A 6) is not relevant. One also usually makes the assumption that $\beta = \gamma$ to limit the number of constants (de Borst 1991). The square root of the ratio β/μ has the dimension of length.

For a more complete description of Cosserat mechanics, the reader is referred to the work by Forest (2001).

APPENDIX B

Second-grade continuum

The strain and its gradient are decomposed into their elastic and plastic parts:

$$\varepsilon_{ij} = \varepsilon^{\mathrm{e}}_{ij} + \varepsilon^{\mathrm{p}}_{ij}, \quad \eta_{ijk} = \partial_{x_k}\varepsilon_{ij} = \eta^{\mathrm{e}}_{ijk} + \eta^{\mathrm{p}}_{ijk}. \tag{B 1}$$

The associated stresses are the classical Cauchy stress σ_{ij} and the hyperstress tensor m_{ijk}. The following simplified form of the elastic relations has been chosen by Shu and Fleck (1999):

$$\sigma_{ij} = C_{ijkl}\varepsilon^{\mathrm{e}}_{kl}, \quad m_{ijk} = l_{\mathrm{e}}^2 C_{ijpq}\eta^{\mathrm{e}}_{pqk}, \tag{B 2}$$

where the usual four-rank elasticity tensor is denoted by C_{ijkl} and l^{e} is a characteristic length associated with the higher-order elasticity law. For the structure to be in equilibrium, the stress tensors must fulfil the following balance equation:

$$\partial_{x_j}\sigma_{ij} - \partial_{x_j x_k} m_{ijk} = 0, \tag{B 3}$$

where volume single and double forces have been excluded. Note that equilibrium is governed by a single higher-order partial differential equation whereas two balance

equations must be fulfilled for the Cosserat continuum. For this continuum, a boundary value problem is well-posed provided that boundary conditions are prescribed to one element in each pair (u_i, t_i) and $(\mathrm{D}u_i, r_i)$. The unknown displacement is denoted by u_i and $\mathrm{D}u_i$ is the normal gradient of u_i defined by

$$\mathrm{D}u_i = (\partial_{x_j} u_i) n_j \tag{B 4}$$

for a unit vector **n** normal to a surface. The corresponding tangent gradient operator is

$$\mathrm{D}_j(.) = \partial_{x_j}(.) - \mathrm{D}(.) n_j. \tag{B 5}$$

The traction vector **t** and double-traction vector **r** on a surface element of normal **n** are respectively defined by

$$t_i = (\sigma_{ij} - \partial_{x_k} m_{ijk}) n_j + (\mathrm{D}_l n_l) m_{ijk} n_j n_k - \mathrm{D}_j (m_{ijk} n_k), \tag{B 6}$$

$$r_i = m_{ijk} n_j n_k. \tag{B 7}$$

In the case of single slip in a system $(\mathbf{s}, \boldsymbol{\nu})$ (slip direction **s** and slip plane normal $\boldsymbol{\nu}$), the plastic strain and strain gradient are related to the amount of slip γ^{p} and the slip gradient variable γ^{S} by

$$\dot{\varepsilon}^{\mathrm{p}}_{ij} = \dot{\gamma}^{\mathrm{p}} s_{(i} \nu_{j)}, \quad \dot{\eta}^{\mathrm{p}}_{ijk} = \dot{\gamma}^{\mathrm{S}} s_{(i} \nu_{j)} s_k, \tag{B 8}$$

where the parentheses around indices stand for symmetrization. Note that, in the general theory proposed by Shu and Fleck (1999), additional slip gradient variables γ^{T} and γ^{M} are introduced that we do not include in the simple case investigated here. It must be noted also that in this theory the slip gradient variable γ^{S} does not necessarily coincide with the gradient of slip γ^{p}.

The plastic yield criterion is a generalized Schmid law involving resolved shear stresses and hyperstresses:

$$\sigma_{\mathrm{eq}} = |\tau| + \frac{|m|}{l_{\mathrm{p}}},$$

with

$$\tau = \sigma_{ij} s_i \nu_j, \quad m = m_{ijk} s_i \nu_j s_k. \tag{B 9}$$

Plastic deformation can then occur when σ_{eq} reaches the threshold τ_{c}. Shu and Fleck (1999) proposed a viscoplastic formulation of the constitutive framework. In contrast, an elastoplastic formulation is used here, for the simple case of single slip. Associative plastic flow is assumed. Thus, the normality rule is given as

$$\dot{\gamma}^{\mathrm{p}} = \dot{q}\, \partial_{\tau} \sigma_{\mathrm{eq}} = \dot{q}\, \mathrm{sgn}\, \tau, \tag{B 10}$$

$$\dot{\gamma}^{\mathrm{S}} = \dot{q}\, \partial_{\mathrm{m}} \sigma_{\mathrm{eq}} = \frac{\dot{q}}{l^{\mathrm{p}}}\, \mathrm{sgn}\, m, \tag{B 11}$$

where $\dot{q}$ denotes the plastic multiplier in both equations.

Two characteristic lengths appear in the theory, namely l^{e} in equations (B 2) and l^{p} in equation (B 9).

References

Acharya, A., and Bassani, J. L., 2000, *J. Mech. Phys. Solids*, **48**, 1565.
Acharya, A., and Beaudoin, A. J., 2000, *J. Mech. Phys. Solids*, **48**, 2213.

Aifantis, E. C., 1987, *Int. J. Plasticity*, **3**, 211; 1999, *J. Engng Mater. Technol.*, **121**, 189.
Asaro, R. J., 1983, *J. Appl. Mech.*, **50**, 921.
Ashby, M. F., 1970, *Phil. Mag.*, **21**, 399.
Bassani, J. L., Needleman, A., and Van der Giessen, E., 2001, *Int. J. Solids Struct.*, **38**, 833.
Busso, E. P., Meissonnier, F. T., and O'Dowd, N. P., 2000, *J. Mech. Phys. Solids*, **48**, 2333.
Cleveringa, H., Van der Giessen, E., and Needleman, A., 1998, *J. Phys., Paris, IV*, **8**, Pr4-83.
de Borst, R., 1991, *Engng Comput.*, **8**, 317.
Devincre, B., Kubin, L., Lemarchand, C., and Madec, R., 2001, *Mater. Sci. Engng*, **A309–A310**, 211.
Estrin, Y., Sluys, B., Bréchet, Y., and Molinari, A., 1998, *J. Phys., Paris, IV*, **8**, Pr8-135.
Fleck, N. A., and Hutchinson, J. W., 1997, *Adv. appl. Mech.*, **33**, 295.
Forest, S., 2001, *Encyclopedia of Materials: Science and Technology*, edited by K. H. J. Buschow, R. W. Cahn, M. C. Flemings, B. Ilschner, E. J. Kramer and S. Mahajan (Amsterdam: Elsevier), pp. 1715–1718.
Forest, S., Barbe, F., and Cailletaud, G., 2000, *Int. J. Solids Struct.*, **37**, 7105.
Forest, S., Dendievel, R., and Canova, G. R., 1999, *Modelling Simulation Mater. Sci. Engng*, **7**, 829.
Forest, S., Pradel, F., and Sab, K., 2001a, *Int. J. Solids Struct.*, **38**, 4585.
Forest, S., van der Giessen, E., and Kubin, L. (editors), 2001b, *J. Phys., Paris, IV*, **11**, Pr5.
Friedman, L. H., and Chrzan, D. C., 1998, *Phil. Mag.* A, **77**, 1185.
Germain, P., 1973, *J. Méc.*, **12**, 235.
Hirth, J. P., and Lothe, J., 1982, *Theory of Dislocations* (New York: Wiley–Interscience).
Huang, J., Kalaitzidou, K., Sutherland, J. W., Milligan, W. W., Aifantis, E. C., Sievert, R., and Forest, S., 2001, *Proceedings of the Fourth International ESAFORM Conference on Material Forming*, Université de Liège, Belgium, 2001, edited by A.-M. Habraken, pp. 527–536.
Koiter, W. T., 1963, *K. Ned. Akad. Wetenschappen., Proc.*, B, **67**, 17.
Kröner, E., 1956, *Z. Naturforschg.*, **11a**, 969.
Kubin, L. P., Canova, G., Condat, M., Devincre, B., Pontikis, V., and Bréchet, Y., 1992, *Solid St. Phenomena*, **23–24**, 455.
Mandel, J., 1973, *Int. J. Solids Struct.*, **9**, 725.
Méric, L., Poubanne, P., and Cailletaud, G., 1991, *J. Engng Mater. Technol.*, **113**, 162.
Mindlin, R. D., and Eshel, N. N., 1968, *Int. J. Solids Struct.*, **4**, 109.
Mughrabi, H., 1983, *Acta metall.*, **31**, 1367; 2001, *Mater. Sci. Engng*, **A317**, 171.
Sedláček, R., and Forest, S., 2000, *Phys. Stat. soli.* (b), **221**, 583.
Sedláček, R., Kratochvíl, J., and Werner, E., 2003, *Phil. Mag.* A (submitted).
Shu, J. Y., and Fleck, N. A., 1999, *J. Mech. Phys. Solids*, **47**, 297.
Shu, J. Y., Fleck, N. A., Van der Giessen, E., and Needleman, A., 2001, *J. Mech. Phys. Solids*, **49**, 1361.
Tanaka, K., and Mura, T., 1981, *J. appl. Mech.*, **48**, 97.